

PAPER • OPEN ACCESS

Study on formability and strain hardening index: influence of particle size of boron carbide (B_4C) in magnesium matrix composites fabricated by powder metallurgy technique

To cite this article: P R Rajkumar *et al* 2020 *Mater. Res. Express* 7 016597

View the [article online](#) for updates and enhancements.

Recent citations

- [Influence of Optimization Techniques on Wire Electrical Discharge Machining of Ti-6Al-2Sn-4Zr-2Mo Alloy using Modeling Approach](#)
A. Perumal *et al*
- [Machinability of Titanium alloy 6242 by AWJM through Taguchi method](#)
A. Perumal *et al*
- [Evaluation of EDM process parameters on titanium alloy through Taguchi approach](#)
A. Perumal *et al*



The Electrochemical Society
Advancing solid state & electrochemical science & technology
2021 Virtual Education

Fundamentals of Electrochemistry:
Basic Theory and Kinetic Methods
Instructed by: **Dr. James Noël**
Sun, Sept 19 & Mon, Sept 20 at 12h–15h ET

Register early and save!



Materials Research Express



PAPER

OPEN ACCESS

RECEIVED
18 October 2019

REVISED
2 January 2020

ACCEPTED FOR PUBLICATION
15 January 2020

PUBLISHED
27 January 2020

Original content from this work may be used under the terms of the [Creative Commons Attribution 4.0 licence](#).

Any further distribution of this work must maintain attribution to the author(s) and the title of the work, journal citation and DOI.



Study on formability and strain hardening index: influence of particle size of boron carbide (B_4C) in magnesium matrix composites fabricated by powder metallurgy technique

P R Rajkumar¹, C Kailasanathan¹ , A Senthilkumar¹, N Selvakumar² and A JohnRajan³

¹ Centre for Materials Research, Department of Mechanical Engineering, Sethu Institute of Technology, Pulloor, Kariapatti, Virudhunagar District, Tamil Nadu, India

² Department of Mechanical Engineering, MepcoSchlenk Engineering College, Sivakasi, Virudhunagar District, Tamil Nadu, India

³ Department of Manufacturing Engineering, School of Mechanical Engineering, Vellore Institute of Technology, Vellore, Tamil Nadu, India

E-mail: uthrakailash@yahoo.co.in

Keywords: cold upsetting, triaxial stress, formability, ludwik equation, instantaneous strain hardening, workability

Abstract

In the present investigation, Magnesium composites have been fabricated with boron carbide (B_4C) as reinforcement by powder metallurgical technique. Two different particle sizes—micro and nano B_4C particles with weight percentage of 0%, 5% and 10% has been studied. The green compacts were prepared by cold pressing and then sintering the specimens before being subjected to cold upsetting under triaxial stress state condition in order to study the phenomenon of workability and instantaneous strain hardening index. Powder characterizations are discussed using x-ray Diffraction peaks, Scanning Electron Microscope images and Energy Dispersive Spectrum analysis. Cold upsetting has been preferred to investigate the performance of the composites. The values of formability stress index factor (β_σ), various stress ratio ($\sigma_\theta/\sigma_{eff}$, σ_m/σ_{eff} and σ_z/σ_m) parameters and instantaneous strain hardening index (n_i) are observed for increase in % of B_4C particles and its sizes. The experimental results were analyzed pertaining to relative density. The results reveal that Mg-10% nano B_4C composite has higher relative density, formability stress index factor and hence high workability than the other composites. The addition of B_4C particles as reinforcement affects the strain hardening index due to geometric and work hardening of the composites.

1. Introduction

Metal Matrix Composites (MMCs) which comprise wide choice of materials were meant to achieve predominant properties than unreinforced monolithic metals have seen a lot of improvement for a long time because of their promising propelled properties [1]. Although the matrix may be of an alloy or a metal, mechanical properties being the primary objective can be improved by selecting the light structural metals for hybrid metal matrix composites and improvements has been made in the reinforcements used [2].

The lightest among metals—Magnesium and its alloys, which possess low density, high specific strength, modulus, stiffness, better castability and weldability, become the appealing material for applications in aerospace and automobile sectors and also machinability can be improved with the utilization of discontinuous particle reinforcements. The density of magnesium is relatively lower than aluminium and further far lower than steel [3–5]. Anyhow, Mg alloys have deficient high temperature strength and worst corrosion resistance which limit their applications that can be enhanced by reinforcing the particles in the magnesium matrix [6]. Generally different grades of Magnesium such as AZ31, AZ61, AZ91 and ZM21 are used as base metals and the reinforcements such as nitrides, carbides, oxides and borides can be used for preparing magnesium composites [7–9]. Emerging need for lightweight materials with particular properties catalysed considerable interest towards development of numerous high performance composite materials. Reinforcements usually comprise of

particles or whiskers with even small volume fractions greatly improve the strength and stiffness of the composites [10].

Among various reinforcements used with magnesium, boron carbide (B_4C) is the best because of its low density combined with high hardness, fracture toughness, superior elastic modulus and tremendous wear resistance [11, 12]. Because of its better properties, it has extensive applications in nuclear, automobile and aerospace sectors and high skilled applications such as light weight shields, fast-breeders, abrasive grit, and nozzles, cutting and grinding tools and so on [13–15].

The popularity of magnesium matrix composites in day-to-day life is delayed because of the cost, which mainly involves the cost of reinforcement particles and the method of fabrication [16]. Hence the potential of magnesium matrix composites with wide variety of reinforcing materials in advanced functional and structural materials needs attention in processing techniques and their features in order to select the suitable fabrication technique for that particular composite material. To fabricate magnesium matrix composites, three well-known processing techniques namely Powder Metallurgy (P/M), squeeze casting and stir casting are available [17]. The P/M technique is attractive among others because particles reinforced were evenly distributed in the matrix thereby regulating the microstructure and improving the structural and mechanical properties [18].

Al–SiC composites subjected to mechanical, machinability and metallurgical studies reveals that reducing the size of the particle reinforcement increases the life in low cycle fatigue because of cyclic hardening [19]. Relative density of the composite materials increases monotonically with pressure [20]. Cyclic stress response of the composite materials relies on the selection of reinforcement's weight percentage and its particle size. Al–SiC composites subjected to upsetting test reveal that the formability of the composites was better compared to pure aluminium. Decreasing the aspect ratio of the composites gives better formability stress index rate because of the high densification [21].

Workability is defined as the capability of the composite material to resist the deformation sustaining the interior stresses before the crack initiation takes place leading to failure during cold upsetting [22]. Studies on powder metallurgy composites for its workability behaviour [23] reveals the investigation of the influence of relative density with formability stress index (β_σ) to describe the influence of the effective and mean stresses with the help of Kuhn-Downey and Whang-Kobayashi theories. Strain hardening is a process of permanent plastic deformation triggered by the phenomenon of slip then by the dislocations generated and its interactions. The behaviour of strain hardening of the sintered powder metallurgy composites Al– Al_2O_3 and Al–Fe during cold upsetting performed under uniaxial, biaxial and triaxial stress state conditions was investigated by Narayanasamy *et al* [24–28]. Jabbari-Taleghani *et al* [29] investigated hot workability behaviour of AZ91 Mg alloy and reveals that it has high hardness of (133 HV) and crystallite size around 150 nm. Zhou *et al* [30] observed the hot deformation behaviour of the stir casted Mg–SiC particulate composites and investigated with processing maps which has lots of applications in aerospace and automobile parts due to its good tensile and compressive strength.

Workability assesses the performance capacity to absorb the generation of internal stresses against the crack initiation and propagation leading to failure and furthermore its plastic deformation. Increasing the relative density increases the plastic deformation of the composites [31, 32]. Workability of the composites subjected to triaxial stress state of condition can be accessed from effective stress and mean stress values whereas the mean stress can be calculated from hoop and axial stress values [33]. The workability relies upon the reinforcement particle size, its weight percentage in the matrix and also the aspect ratio of the composites. Further the relative density, stress-strain rate also influences the workability [34, 35]. The crack initiation relying on mean stress [36] was proved from the correlation between the triaxial stresses and its strain and formability stress index factor (β_α) also determined to analyse the influence of mean and effective stress (σ_m and σ_{eff}) [37].

Increasing the percentage by weight of particle reinforcements enhances the compressibility of the composites [38]. Selvakumar *et al* [22, 39] reveals that the workability of the composites subjected to triaxial stress state condition by analysing the influence of various stresses pertaining to relative density and concluded that increasing the percentage of particle reinforcements increases the workability because of the increase in relative density. Preforms that possess high workability have high relative density and low aspect ratio. Different tests like hardness, tensile etc, were conducted on the composites to investigate its mechanical behaviour. Reinforcement type and its composition play a vital role in the strain hardening of composite materials [40].

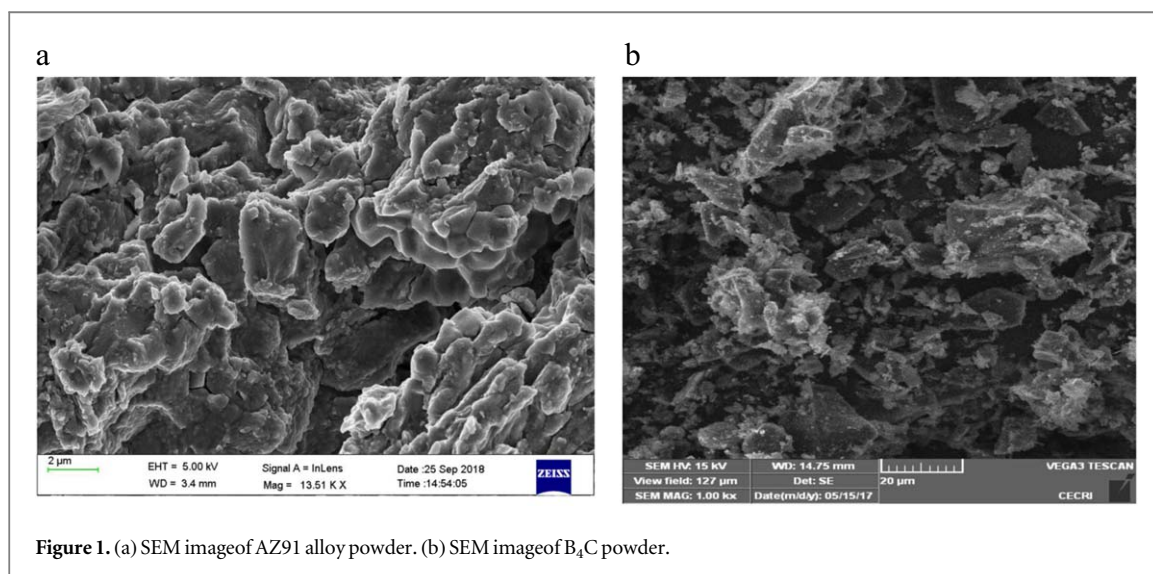
To the authors' knowledge, literature related to workability during cold upsetting of Mg– B_4C nano composites subjected to triaxial stress state of condition by varying the size of the reinforcement particles and its weight percentage are not available. In this present investigation, Mg– B_4C preforms with different particle size and weight percentage has been made by cold upsetting and discussed the influence of varying the size of the particle reinforcement and its weight percentage on the behaviour of workability and instantaneous strain hardening subjected to triaxial stress state of condition. Relative density and its relationship with various stress ratios and its effect with particle size and weight percentage also been discussed.

Table 1. Elemental details of magnesium alloy (AZ91) powder.

Mg	Al	Mn	Zn	Si	Fe
94.72	4.66	0.16	0.44	<0.01	<0.01

Table 2. Elemental details of boron carbide (B_4C) powder.

B	C	O	Si	Fe	Others
69.47	24.51	4.97	0.11	0.05	Bal.

**Figure 1.** (a) SEM image of AZ91 alloy powder. (b) SEM image of B_4C powder.

2. Experimental details

2.1. Materials

In this investigation, the matrix is Magnesium (Mg) AZ91 alloy and it is reinforced with boron carbide (B_4C) of two different particle sizes about 60 microns and 38 nm respectively. The elemental details of both Mg and B_4C are given in tables 1 and 2 respectively. The Mg alloy powder has an average particle size of 70 microns. The weight percentage of B_4C powder is selected as 5% and 10% respectively and the preforms were prepared by powder metallurgy route.

2.2. Material characterization

Magnesium alloy (AZ91) and B_4C powder has been characterised for morphological study using Scanning Electron Microscope (SEM) images. Figure 1(a) shows the SEM image of Mg AZ91 alloy. It has ellipsoidal and spherical structure with particle size of around 70 μm . Figure 1(b) shows the SEM images of B_4C powder. It looks like a polygonal structure.

The crystal structure, phase identification and the presence of particle is measured and confirmed using x-ray Diffractometer (XRD) peaks. The x-rays was produced from anode material $CuK\alpha_1$ which has a wavelength of 1.54060 \AA to obtain the diffraction patterns of the Mg AZ91 alloy and B_4C powder. figures 2(a) and (b) illustrates the XRD patterns and peaks of Mg AZ91 alloy and B_4C powder. The measurement conditions of the test have 2θ angle with scan angle from $10^\circ - 80^\circ$ with step size of 0.017° . The average crystal size of nano B_4C powder obtained from ball milling was calculated from Deybe-Scherrer equation as 38 nm. The crystal peaks are also identified from the XRD analysis. The XRD patterns were drawn between 2θ and intensity (arbitrary unit). The crystalline structure of the as received Mg alloy powder has been determined as shown in figure 2(a) which indicates the high peaks for particular intensity at 2θ values of 32.51° , 34.77° , 37.02° , 48.35° , 57.89° , 63.61° , 70.37° and 73.10° with crystal planes (1 0 0), (0 0 2), (1 0 1), (1 0 2), (1 1 0), (1 0 3) and (2 0 1) respectively. The lattice parameters was determined to be $a = 3.1768 \text{\AA}$ and $c = 5.1781 \text{\AA}$ which reasonably agrees with the standard JCPDS card number 89-5003 with $a = 3.208 \text{\AA}$ and $c = 5.209 \text{\AA}$ of hexagonal structure. Similarly, the crystalline structure of the as received B_4C powder has been determined from figure 2(b) which shows the high peaks for particular intensity at 2θ values of 19.73° , 22.10° , 23.53° , 31.96° , 34.99° , 37.82° , 39.18° ,

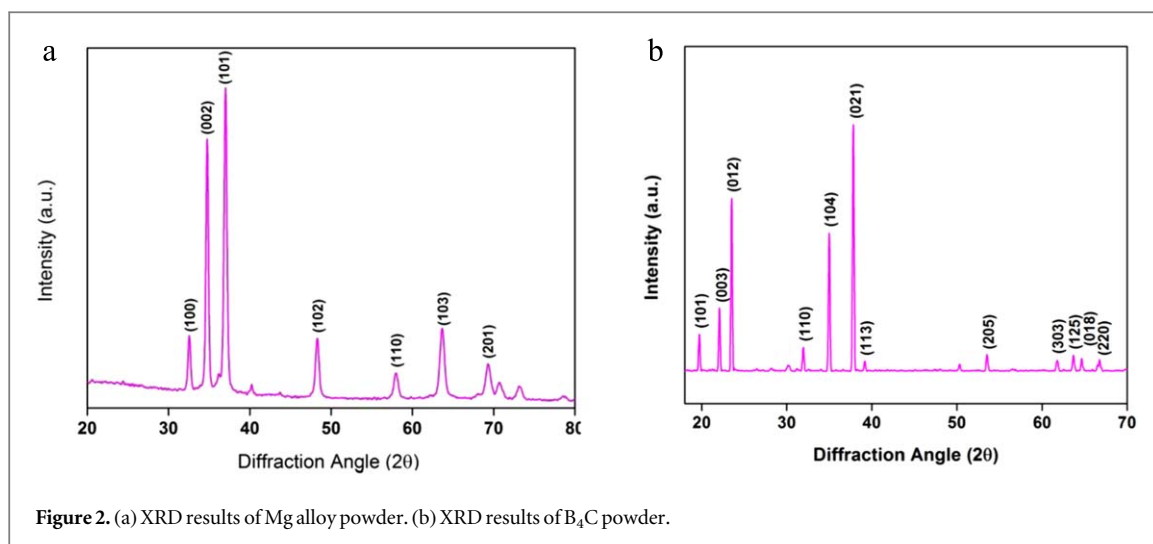


Figure 2. (a) XRD results of Mg alloy powder. (b) XRD results of B_4C powder.

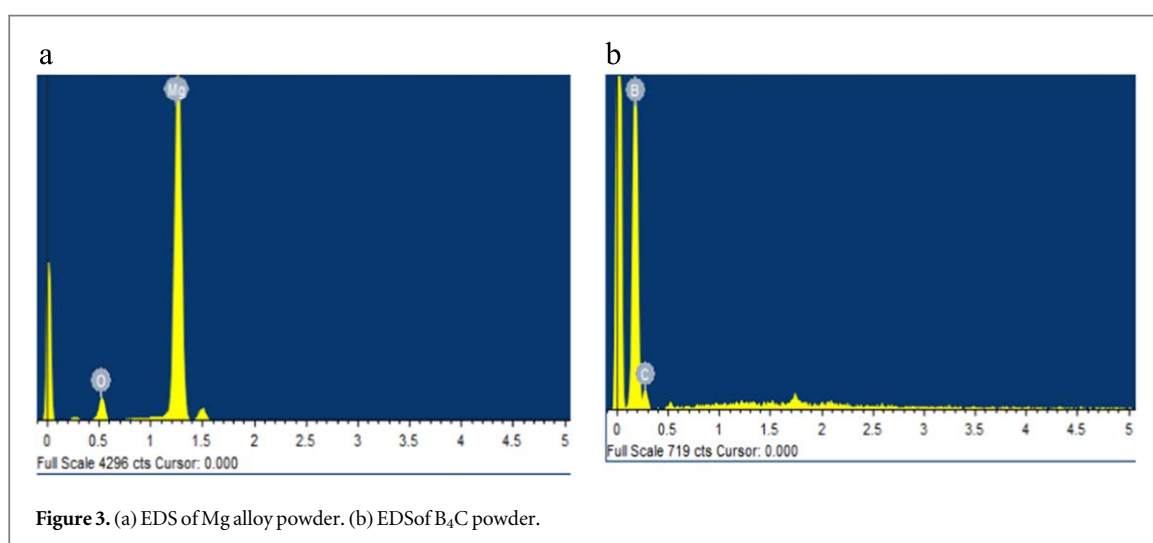


Figure 3. (a) EDS of Mg alloy powder. (b) EDS of B_4C powder.

53.50°, 61.79°, 63.68°, 64.63° and 66.79° with crystal planes (1 0 1), (0 0 3), (0 1 2), (1 1 0), (1 0 4), (0 2 1), (1 1 3), (2 0 5), (3 0 3), (1 2 5), (0 1 8) and (2 2 0) respectively. The lattice parameters almost match with the standard JCPDS card number 35-0798 with $a = 5.600 \text{ \AA}$ and $c = 12.086 \text{ \AA}$ having a rhombohedral crystallographic structure.

The element peaks and its chemical composition of Mg AZ91 alloy and B_4C powder are confirmed through Energy Dispersive Spectrometer (EDS) analysis. Figures 3(a) and (b) illustrates the elemental (EDS) analysis of Mg AZ91 alloy and B_4C powder. It shows the existence of Mg at an intensive signal of around 1.25 keV. Boron and carbon has an intensive signal at 0.2 keV and 0.30 keV respectively. Boron has higher elemental composition, hence it has highest peak than carbon.

2.3. Preparation of composites

2.3.1. Blending

The primary matrix (Mg) and as received reinforcement particles (B_4C) were blended using planetary ball mill which has 10 mm diameter tungsten carbide balls and hybridize each other to distribute the secondary phase particles homogeneously on the matrix. Since Magnesium alloy is highly reactive with atmosphere, the ball milling was performed under protective argon atmosphere to prevent oxidation during the process and the powder was handled carefully during loading and unloading. In the present investigation, reinforcement is added in the weight percentage of 5% and 10% respectively. Each blending has been done at 150 rpm for two hours. Initially, the planetary ball mill was used with the ball to powder ratio of 20:1 at 200 rpm for 30 h to synthesise B_4C powder separately. Milling was done intermittently to overcome the frictional heat by using toluene as the process control agent. Finally after 30 h of milling, the size of the particles was measured and characterized using SEM and XRD. The final mean size of the particle is 38 nm. This B_4C powder particle is then blended with Mg as said above with the same weight percentage of 5% and 10% respectively.

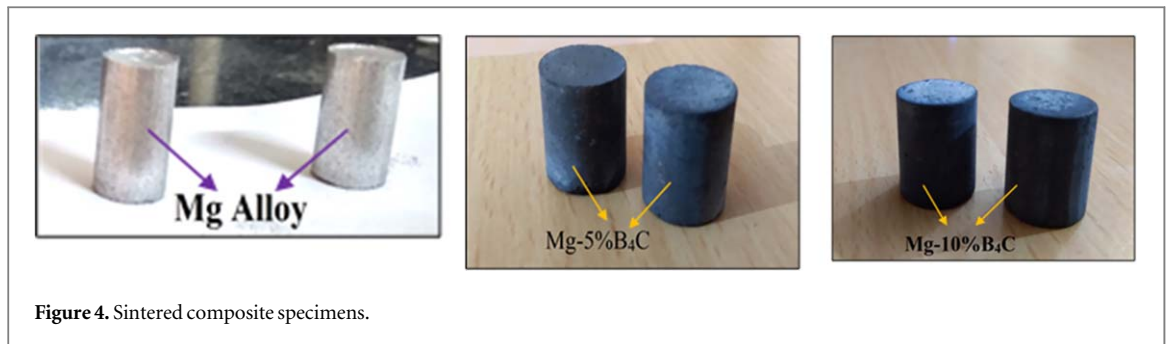


Figure 4. Sintered composite specimens.

2.3.2. Compaction

The blended powders were heated to 120 °C for 2 h in the furnace to eradicate the unstable matters present in it. Then the dried blended powder is filled into the die and then compacted by gradually applying the uniaxial compressive load in the hydraulic press up to a pressure of 550 MPa and then removed the green compact specimen safely from the die. Zinc stearate has been used for die wall lubrication before each run. The green compacted specimen was prepared with a diameter of 10 mm and height 10 mm respectively for all the combinations.

2.3.3. Sintering

The green compacts are then subjected to the sintering process. Sintering was done in a controlled atmosphere tubular furnace at the temperature of 520 °C with a dwell time of 1 h and allowed to get cooled inside the furnace itself. The sintered samples cannot be used directly for characterization study because of their hard surfaces. Hence the surfaces should be polished for microscopic analysis. The sintered composite specimens are shown in figure 4.

2.4. Characterization of composites

To study about the characterization of composites, the sintered composite specimen end surfaces were cleaned and polished in succession with the SiC abrasive papers of fine grit sizes 600, 800 and 1000 respectively in the disc polishing machine to get a mirror-like surface finish. Then the polished composite specimens were etched as per the metallographic study and examined for their characterization.

The SEM images of the sintered composites with Mg – 5% B₄C and Mg – 10% B₄C shown in figures 5(a) and (c) respectively illustrate the even distribution of reinforcement particles in the Magnesium matrix. The structure of the composites shows the mixture of flake shapes along with polygonal shapes of different sizes because of the clustering of the B₄C reinforcement particles with Mg matrix.

The EDS analysis of the same specimens is shown in figures 5(b) and (d) respectively. From the images the presence of magnesium (Mg) and boron carbide (B₄C) particles is confirmed and shows that the elemental peaks of Mg occur at 1.25 keV, boron (B) and carbon (C) at 0.2 keV and 0.30 keV with respect to the cps/eV value. Also, Mg has the highest peak than boron and carbon particles due to its high percentage by weight than others. Increasing from 5% to 10%, the corresponding peaks of boron and carbon also increase in the composites.

X-ray diffraction analysis is also made on the composites to confirm the intensity peaks of the particles. Figures 5(e) and (f) confirm the presence of magnesium (Mg) with higher intensity peaks due to its high weight percentage. The intensity peaks of the B₄C particles increase by increasing their weight percentage (figures 5(e) and (f)). Hence the presence of Mg and B₄C particles was confirmed through XRD analysis and it is identified that increasing the weight percentage of B₄C particles the intensity peak increases. There are no other intermetallic compounds formed during sintering. This was clearly identified from the XRD analysis. This may be attributed to the controlled inert atmosphere maintained in the tubular furnace during sintering.

2.5. Experimentation

2.5.1. Cold upsetting

To study about the cold workability behaviour of the Mg-5% B₄C composites and Mg-10% B₄C composites, a cold deformation test has been carried out. The workability may be defined as the capability of the P/M composite to endure the crack initiation during cold upsetting by means of distortion measurement [22, 37]. Initial specimen dimensions such as diameter (D_o), height (h_o) and theoretical density of the fully dense material (ρ_{th}) are measured. By means of Archimedes' principle, the initial density (ρ_o) of the composites is measured. Then the cold upsetting of the composites has been done in the universal testing machine with 1 MN capacity. Each specimen undergoes the compressive load increasing in the order of 0.01 MN during upsetting. The dimensional changes such as bulged diameter (D_b), contact diameter at the top (D_{CT}) and bottom (D_{CB}),

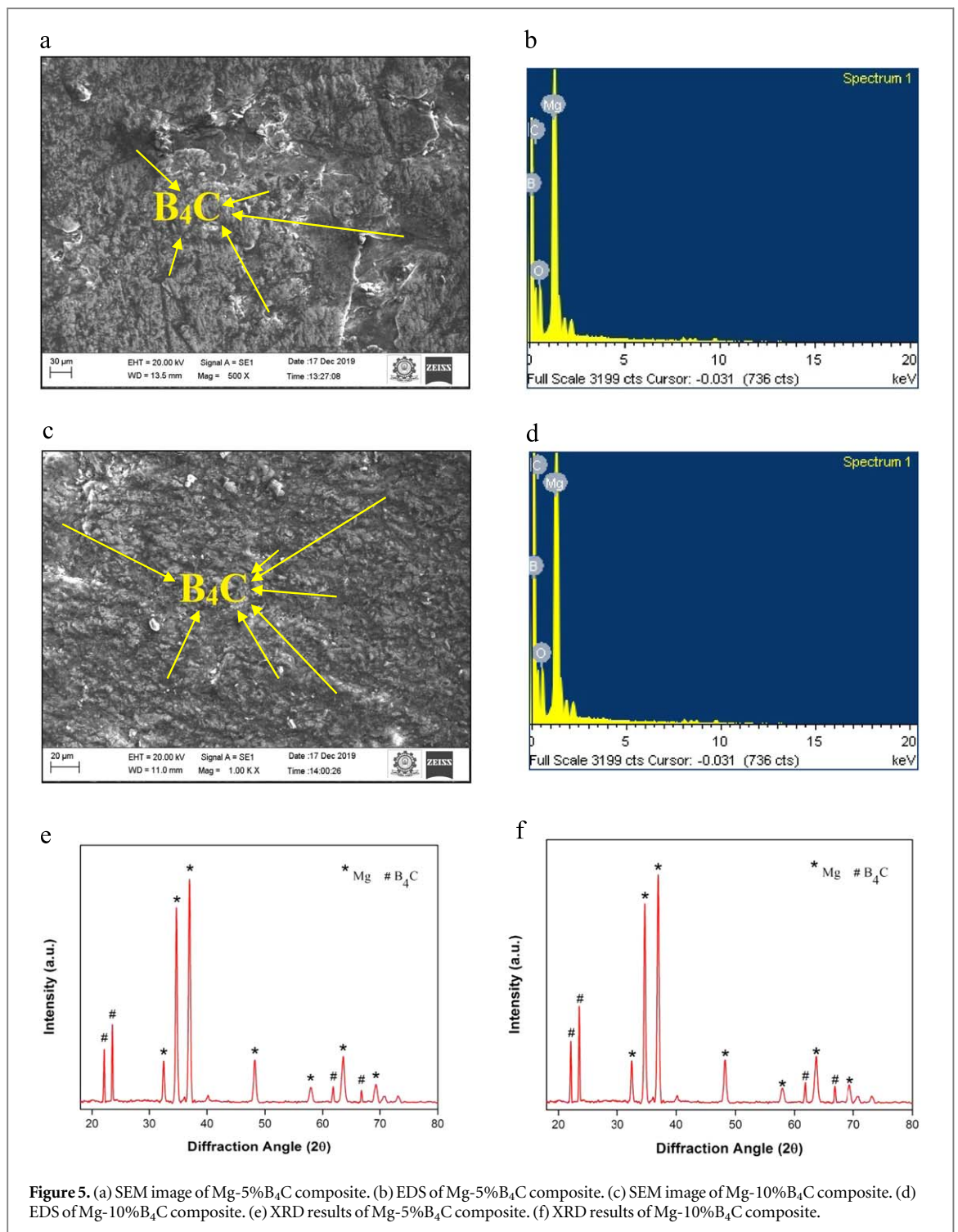


Figure 5. (a) SEM image of Mg-5%B₄C composite. (b) EDS of Mg-5%B₄C composite. (c) SEM image of Mg-10%B₄C composite. (d) EDS of Mg-10%B₄C composite. (e) XRD results of Mg-5%B₄C composite. (f) XRD results of Mg-10%B₄C composite.

specimen height (h_f) and density of the composites after deformation (ρ_f) are measured. The incremental load is applied until the initial crack has been detected on the free surface of the specimen. The contact diameter (D_c) and the relative density (R) of the specimens are also calculated. The formability stress index factor (β_σ) is calculated from the triaxial hydrostatic and effective (σ_m and σ_{eff}) stresses which defines the workability behaviour of the composites. The schematic illustration of an upset forming- before and after deformation has been explained in the figure 6 [41].

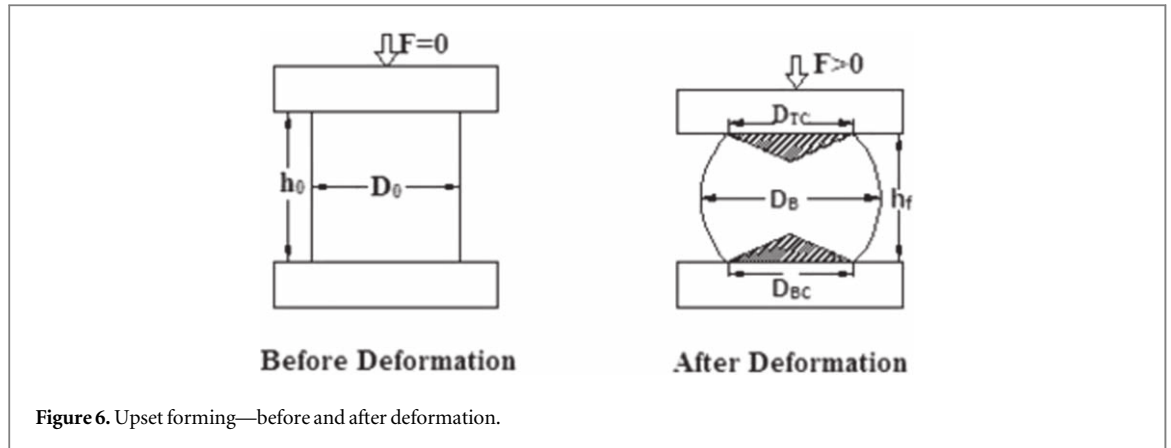


Figure 6. Upset forming—before and after deformation.

3. Hypothetical investigation

3.1. Measurement of density

Density measurement is needed to study the workability of the composites. The rule of mixture has been used to find out the theoretical densities of the fabricated composites (ρ_{th}) using the equation (1).

$$\rho_{th} = [(\rho_{Mg} \times wt\%_{Mg}) + (\rho_{B_4C} \times wt\%_{B_4C})] \quad (1)$$

where, ρ_{th} , ρ_{Mg} , ρ_{B_4C} refers to the theoretical densities of the completely dense material, magnesium (Mg) and boron carbide (B_4C) respectively in terms of g/cc and $wt\%_{Mg}$, $wt\%_{B_4C}$ refers to the weight percentage of magnesium (Mg) and boron carbide (B_4C).

In keeping with Archimedes principle, the densities of the specimen before (ρ_o) and after (ρ_f) deformation are measured as per the ASTM: B962-13 test procedure [42] using a high precision digital balance. The relative density (R) is defined as the ratio of the density of the deformed composite (ρ_f) to its true density (ρ_{th}) and it can be computed through the equation (2).

$$R = \frac{\rho_f}{\rho_{th}} \quad (2)$$

3.2. Triaxial stress state

Specimens with composition of Mg-5% B_4C and Mg-10% B_4C are tried to undergo normal axial stresses acting in three mutually perpendicular directions to cause volumetric deformation in triaxial state. In case of uniaxial stress state of loading, only one axial stress acts and all other stresses are zero whereas in biaxial stress state of loading, two axial stresses act in two directions and the remaining stresses are zero due to the deformation of the shape. In cold upsetting process, uniaxial as well as biaxial stress conditions cannot be applied since they influence the mechanical flow characteristics of the composites. Therefore, the triaxial stress state conditions are used to study these properties of the composites [43].

The contact area of the deformed composites after upsetting (A_C) can be calculated using the formula as given in equation (3).

$$A_C = \frac{\pi D_C^2}{4} \quad (3)$$

where composites' contact diameter, D_C can be calculated using the formula as given in equation (4).

$$D_C = \frac{(D_{CT} + D_{CB})}{2} \quad (4)$$

where, D_{CT} and D_{CB} refers to the contact diameter at the top and bottom of the composites respectively after cold upsetting.

3.2.1. Stresses and strains referred to triaxial stress state

The several stresses, for example, true axial stress (σ_z), effective stress (σ_{eff}), true hoop stress (σ_θ) and mean stress (σ_m) [42] can be calculated to determine the workability behaviour of the prepared composites. True axial stress is direct stress acting on the specimen caused by the application of the axial load which makes deformation and can be expressed as given in equation (5).

$$\sigma_z = \frac{\text{Load}}{\text{Contact Area}} \quad (5)$$

The three types of strains true axial strain (ε_z), true hoop strain (ε_θ) and conventional hoop strain (ε'_θ) are essential for theoretical investigations of workability studies. The strain calculations are followed as per the standard [44].

The true axial strain (ε_z) represents the deformation of composites caused by axial stress. In case of forming of cylindrical specimen, ε_z was calculated from the following expression.

$$\varepsilon_z = \ln \left[\frac{H_o}{H_f} \right] \quad (6)$$

where, H_o and H_f are the height of specimen before and after deformation respectively.

The true hoop strain (ε_θ) caused by hoop stress is defined as the ratio of change in diameter of cylindrical specimen to its actual diameter. The formula of true hoop strain (ε_θ) for a specimen is given in equation (7) as specified by Narayanasamy *et al* [25].

$$\varepsilon_\theta = \ln \left[\frac{D_c}{D_o} \right] \quad (7)$$

Conventional hoop strain (ε'_θ) is calculated from the equation (8) as given below:

$$\varepsilon'_\theta = \ln \left(\frac{2D_b^2 + D_c^2}{3D_o^2} \right) \quad (8)$$

where D_o and D_c are the initial and average contact diameter of the composites and D_b is the bulged diameter of composites after deformation.

The hoop stress (σ_θ) can be calculated from the Poisson's ratio or stress-strain increment (α). Poisson's ratio (α) is the ratio of the changes in hoop strain to the corresponding axial strain [42]. From the Poisson's ratio (α), the hoop stress (σ_θ) can be obtained from the equation (9) [45].

$$\alpha = \frac{d\varepsilon_\theta}{d\varepsilon_z} = \frac{(2 + R^2)\sigma_\theta - R^2(\sigma_z + 2\sigma_\theta)}{(2 + R^2)\sigma_z - R^2(\sigma_z + 2\sigma_\theta)} \quad (9)$$

where, R , σ_z and σ_θ refers to the relative density, true axial stress and hoop stress respectively.

Hoop stress (σ_θ) also called as circumferential stress acting along the lateral surface area of composites will typically be greater than the true axial stress (σ_z). By calculating Poisson's ratio (α), hoop stress (σ_θ), can be obtained from the expression as given in equation (10).

$$\sigma_\theta = \left[\frac{(2\alpha + R^2)}{(2 - R^2 + 2R^2\alpha)} \right] \sigma_z \quad (10)$$

The mean stress (σ_m) is the mean of three mutually perpendicular axial principal stresses. The mean stress (σ_m) formulae for a cylindrical specimen forming is given in equation (11).

$$\sigma_m = \frac{(\sigma_z + \sigma_r + \sigma_\theta)}{3} \quad (11)$$

Since the axial load applied during cold upsetting is compressive, the true axial stress, σ_z and the other two stresses hoop (σ_θ) and radial (σ_r) will be of compressive and tensile in nature respectively. Narayanasamy *et al* [45] investigated that hoop stress (σ_θ) and radial stress (σ_r) are identical for the specimens subjected to axisymmetric load under triaxial stress state of condition during cold upsetting. Thus the equation (11) becomes

$$\sigma_m = \frac{(\sigma_z + 2\sigma_\theta)}{3} \quad (12)$$

During yielding, the stress increases gradually to a critical point, effective stress (σ_{eff}). The expression for effective stress in case of cylindrical preforms [44] is given in the equation (13)

$$\sigma_{eff} = \left[\frac{\sigma_z^2 + 2\sigma_\theta^2 - R^2(\sigma_\theta^2 + 2\sigma_z\sigma_\theta)}{2R^2 - 1} \right]^{0.5} \quad (13)$$

3.3. Formability stress index factor (β_σ)

Formability is the capability of any composite materials to form or deform without failure. The formability stress index factor (β_σ) depends on the influence of mean and effective stresses during cold upsetting of the composites. Vujovic *et al* [46] proposed the expression for formability stress index factor (β_σ), as given in equation (14):

$$\beta_{\sigma} = \frac{3\sigma_m}{\sigma_{eff}} \quad (14)$$

3.4. Instantaneous strain-hardening index (n_i)

The strain-hardening index (n) is calculated from the conventional Ludwik equation

$$\sigma = K\varepsilon^n \quad (15)$$

where K , σ and ε refers to the strength coefficient, true effective stress and strain respectively. In this work, this index is calculated by rewriting the above equation (15) as shown in the equation (16), keeping that the successive compressive loads are specified as ((1, 2, 3... (m-1), m) [32]. This helps to calculate the strain-hardening parameters under triaxial stress state conditions for the prepared composites.

$$n_i = \frac{\ln\left(\frac{\sigma_m}{\sigma_{m-1}}\right)}{\ln\left(\frac{\varepsilon_m}{\varepsilon_{m-1}}\right)} \quad (16)$$

4. Results and discussion

4.1. Influence of cold deformation test

The outcomes of the Mg alloy, Mg-5% micro B₄C, Mg-10% micro B₄C, Mg-5% nano B₄C and Mg-10% nano B₄C composites subjected to cold deformation was discussed by plotting various graphs for the values obtained through parameters theoretically evaluated [43, 44].

4.1.1. Stress variations pertaining to axial strain

Graphs has been plotted as shown in the figures 7(a)–(e) for the Mg alloy, Mg-5% micro B₄C, Mg-10% micro B₄C, Mg-5% nano B₄C and Mg-10% nano B₄C composites with an aspect ratio of one subjected to cold upsetting at triaxial stress state condition to study the various tri-axial stress behaviours like true axial (σ_z), hoop (σ_{θ}), mean (σ_m) and effective (σ_{eff}) stresses pertaining to axial strain (σ_z). The true axial stress (σ_z), compressive in nature during cold upsetting is negative whereas other stresses are tensile and hence positive.

During cold upsetting with gradual application of load, all the stresses gradually increases with respect to strain because of the resistance against deformation. With increase in load, the stress increases because of the growing relative density (R) value by reducing porosity. The stress-strain curve increases gradually till the crack initiation on the composites. By adding the micro B₄C and nano B₄C particles to the magnesium alloy, the relative density of the composites increases owing to the enhanced load transfer capability of the reinforcement to the matrix and hence decreases the porosity.

It has been observed from the results that, addition of reinforcement B₄C particle increases the true axial stress (σ_z) and the stress further increases by increasing the percentage of B₄C. As the size of the reinforcement B₄C particle gets reduced, the true axial stress (σ_z) and strain (σ_z) increases due to the decrease in pore sizes by the reinforcement B₄C particles and its uniform and effective particle distribution which also increases the relative density under the same compacting pressure. The true axial stress (σ_z) remains higher than the hoop stress (σ_{θ}). The mean stress (σ_m) was minimum and the effective stress (σ_{eff}) was maximum because of the better densification. Hence among these composites the Mg-10% nano B₄C composite withstands more stresses for deformation. The maximum values of stresses (σ_z , σ_m , σ_{θ} and σ_{eff}) for all the composites were given in the table 3.

4.1.2. Influence of axial stress (σ_z) pertaining to relative density (R)

The influence of axial stress (σ_z) on relative density (R) has been observed by plotting the graph for the Mg alloy, Mg-5% micro B₄C, Mg-10% micro B₄C, Mg-5% nano B₄C and Mg-10% nano B₄C composites with an aspect ratio of one as revealed in the figure 8. At the beginning of cold upsetting the relative density (R) increases rapidly due to the closure of pores which will be high at that stage but the axial stress (σ_z) is slowly increased because of low resistance against deformation. As the deformation progresses, the porosity reduces and hence the relative density (R) is slowly increased but axial stress (σ_z) begins to increase marginally. It continues till the initial crack was observed on the specimen.

Hence comparing the results of all these composites, the Mg-10% nano B₄C composite withstands high relative density and hence axial stress. This is because of the B₄C reinforcement, which reduces the porosity and increases the densification of the composites and therefore deformation requires high axial stress (σ_z). The maximum values of relative density (R) and true axial stress (σ_z) for all the composites was given in the table 4.

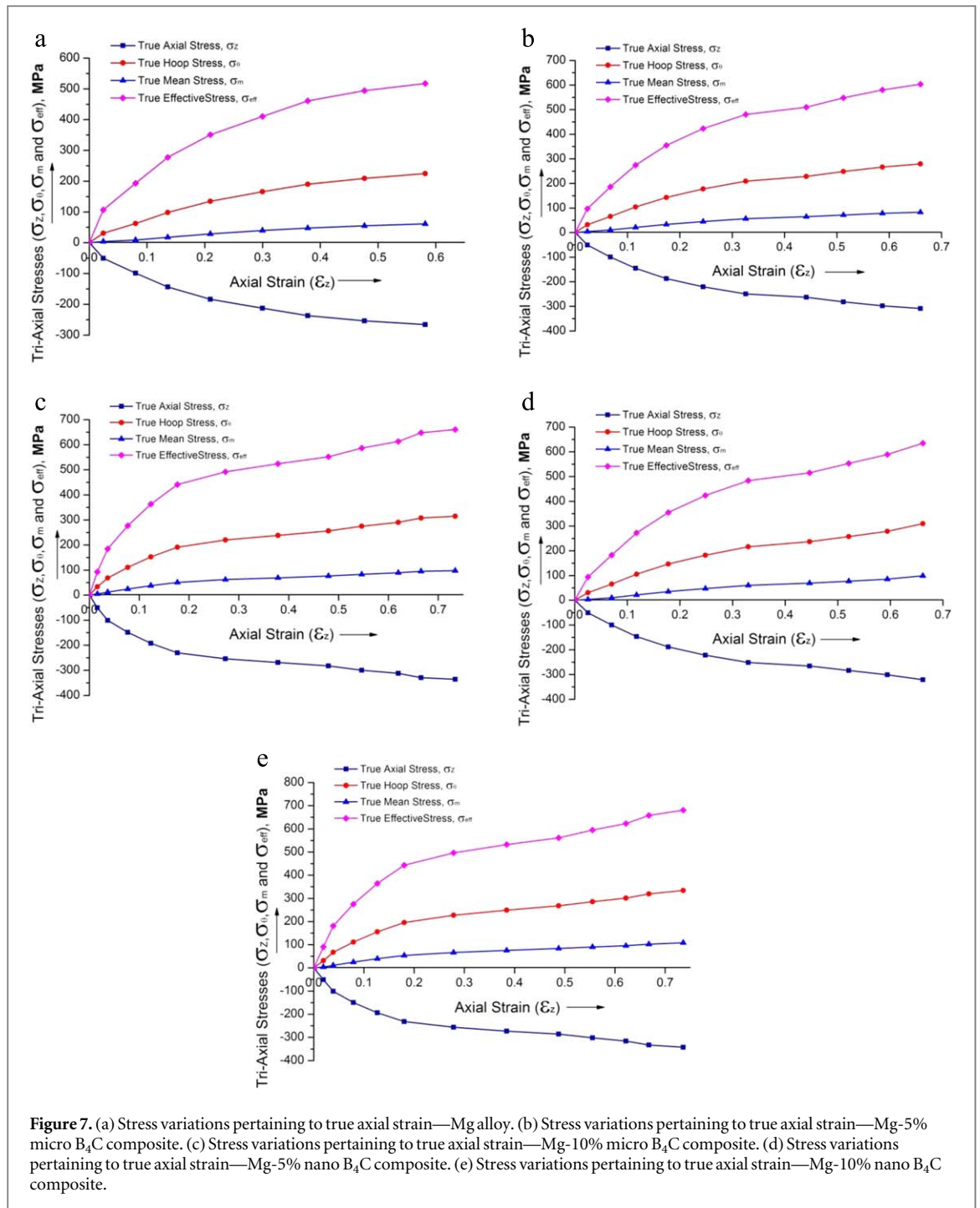


Figure 7. (a) Stress variations pertaining to true axial strain—Mg alloy. (b) Stress variations pertaining to true axial strain—Mg-5% micro B₄C composite. (c) Stress variations pertaining to true axial strain—Mg-10% micro B₄C composite. (d) Stress variations pertaining to true axial strain—Mg-5% nano B₄C composite. (e) Stress variations pertaining to true axial strain—Mg-10% nano B₄C composite.

Table 3. Maximum values of stresses.

S. no.	Stress(MPa)	Composites				
		Mg alloy	Mg-5% micro B ₄ C	Mg-10% micro B ₄ C	Mg-5% nano B ₄ C	Mg-10% nano B ₄ C
1.	Max. Axial stress	265.73	308.79	335.70	321.18	342.78
2.	Max. Hoop stress	224.86	279.16	314.73	309.63	333.91
3.	Max. Mean stress	61.33	83.18	97.92	99.36	108.35
4.	Max. Effective stress	516.99	603.13	660.70	635.04	680.27

4.1.3. Influence of formability stress index (β_σ) pertaining relative density (R)

The relation among formability stress index (β_σ) and relative density (R) for magnesium alloy and its composites containing 5% and 10% B₄C particles of micro and nano sizes is depicted in figure 9. Table 5 shows the

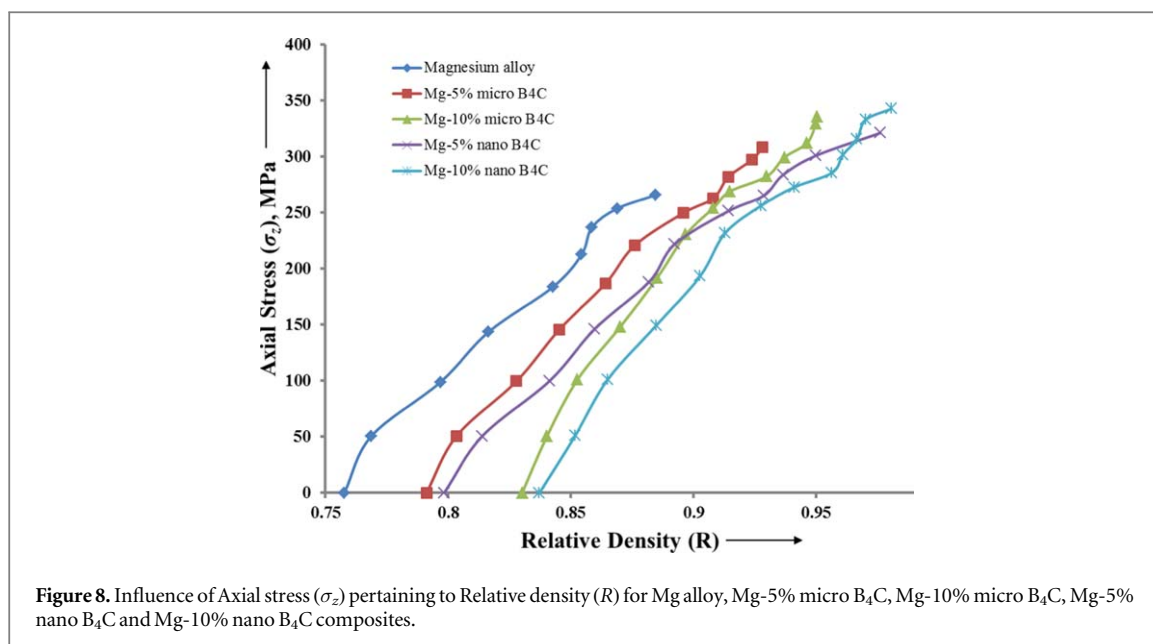
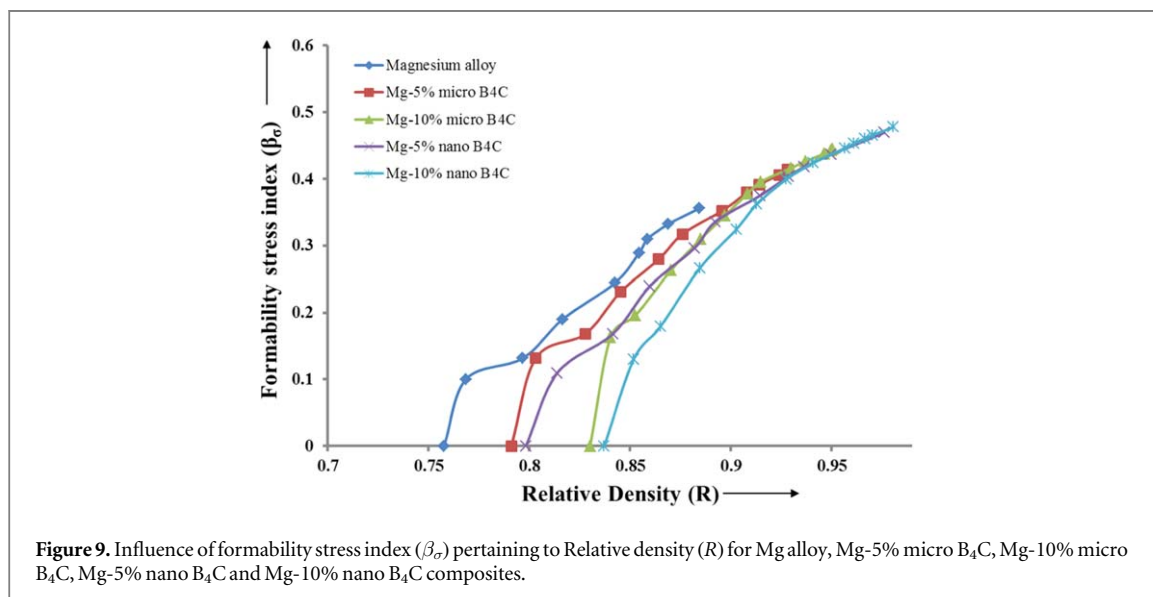


Table 4. The maximum values of relative density (R) and true axial stress (σ_z) for all the composites.

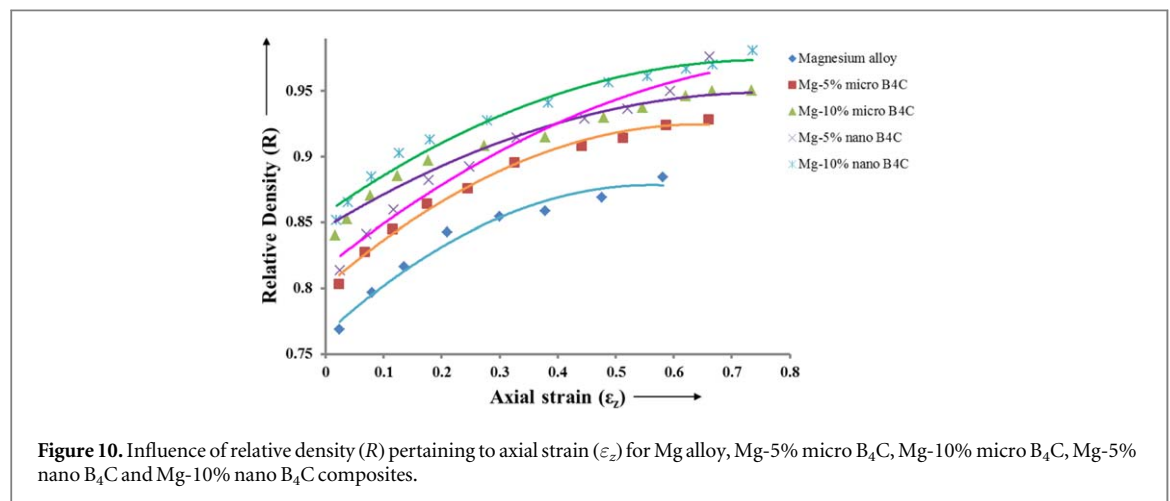
S. no.	Composites	R	σ_z
1.	Mg alloy	0.8845	265.73
2.	Mg-5% micro B_4C	0.9282	308.79
3.	Mg-10% micro B_4C	0.9504	335.70
4.	Mg-5% nano B_4C	0.9761	321.18
5.	Mg-10% nano B_4C	0.9807	342.78



maximum formability stress index (β_σ) values for all composites. It has been observed that reinforcing the B_4C particles into the Mg alloy increases the relative density which in turn reduces the porosity. The same has been observed by reducing the size of the B_4C particles. Thus the formability stress index (β_σ) increases uniformly with relative density (R) with rise in weight percentages of B_4C particles and also by reducing its particle sizes. Relative density increases the workability of composites. During cold upsetting, the relative density is increased because of the increase in density of the composites by reducing porosity. Results shows that Mg-10% nano B_4C composite has high relative density (R) and hence high formability stress index (β_σ) than the other composites.

Table 5. The maximum formability stress index (β_σ) values for all the composites.

S. no.	Composites	β_σ
1.	Mg alloy	0.3559
2.	Mg-5% micro B ₄ C	0.4245
3.	Mg-10% micro B ₄ C	0.4493
4.	Mg-5% nano B ₄ C	0.4524
5.	Mg-10% nano B ₄ C	0.4719

**Figure 10.** Influence of relative density (R) pertaining to axial strain (ϵ_z) for Mg alloy, Mg-5% micro B₄C, Mg-10% micro B₄C, Mg-5% nano B₄C and Mg-10% nano B₄C composites.**Table 6.** The maximum values of axial strain (ϵ_z) for all the composites.

S. no.	Composites	ϵ_z
1.	Mg alloy	0.5816
2.	Mg-5% micro B ₄ C	0.6597
3.	Mg-10% micro B ₄ C	0.7340
4.	Mg-5% nano B ₄ C	0.6616
5.	Mg-10% nano B ₄ C	0.7361

4.1.4. Influence of relative density (R) pertaining to axial strain (ϵ_z)

Figure 10 shows the relation between relative density (R) and axial strain (ϵ_z) for magnesium alloy and its composites containing 5% and 10% B₄C particles of micro and nano sizes by using parabolic curve fitting technique of second order polynomial equation. It has been observed that the relative density (R) increases due to the increasing axial strain (ϵ_z) for all the composites. Initially the relative density increases and becomes consistent with the development of axial strain (ϵ_z). The Mg-10% nano B₄C composite has higher axial strain (ϵ_z). For a particular axial strain (ϵ_z), the relative density increases with the addition of B₄C particles and further improved by reducing the particle sizes. The maximum value of axial strain (ϵ_z) for all the composites are given in the table 6.

4.1.5. Impact of formability stress index (β_σ) pertaining to axial strain (ϵ_z)

Formability stress index (β_σ) graph is plotted against axial strain (ϵ_z) as shown in the figure 11. for magnesium alloy and its composites containing 5% and 10% B₄C particles of micro and nano sizes by using parabolic curve fitting technique of second order polynomial equation. It has been observed that with increasing axial strain (ϵ_z), relative density (R) increases and hence formability stress index (β_σ) increases for all the composites, which is attributed due to the reduction of pores during cold upsetting. The highest values of the formability stress index (β_σ) attained for the Mg alloy, Mg-5% micro B₄C, Mg-10% micro B₄C, Mg-5% nano B₄C and Mg-10% nano B₄C composites are given in the table 5 which shows that Mg-10% nano B₄C composite has the highest value of 0.4719.

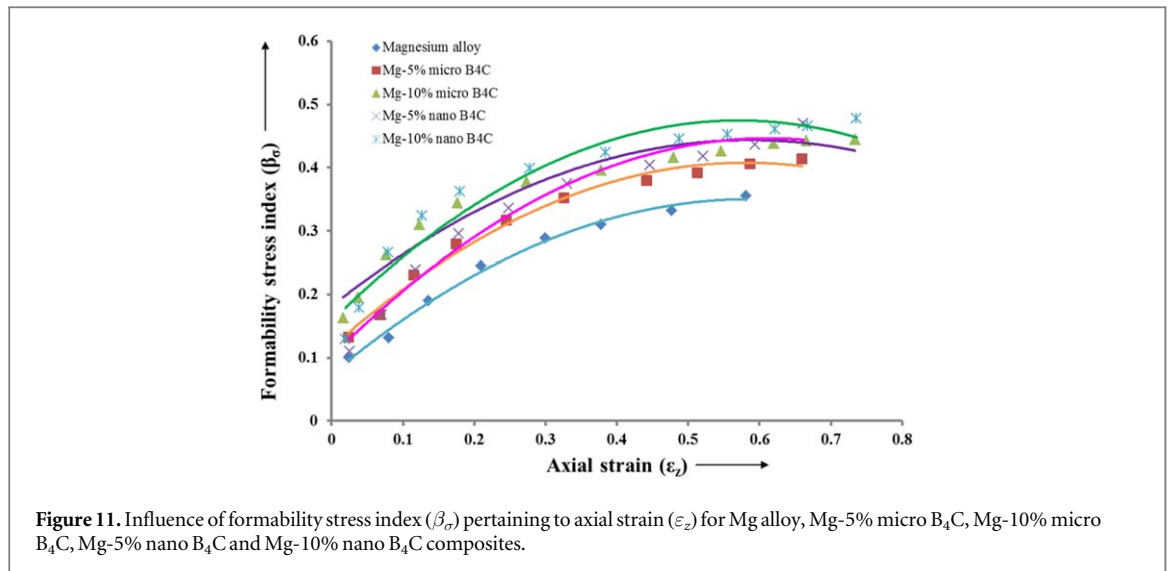


Figure 11. Influence of formability stress index (β_{σ}) pertaining to axial strain (ε_z) for Mg alloy, Mg-5% micro B_4C , Mg-10% micro B_4C , Mg-5% nano B_4C and Mg-10% nano B_4C composites.

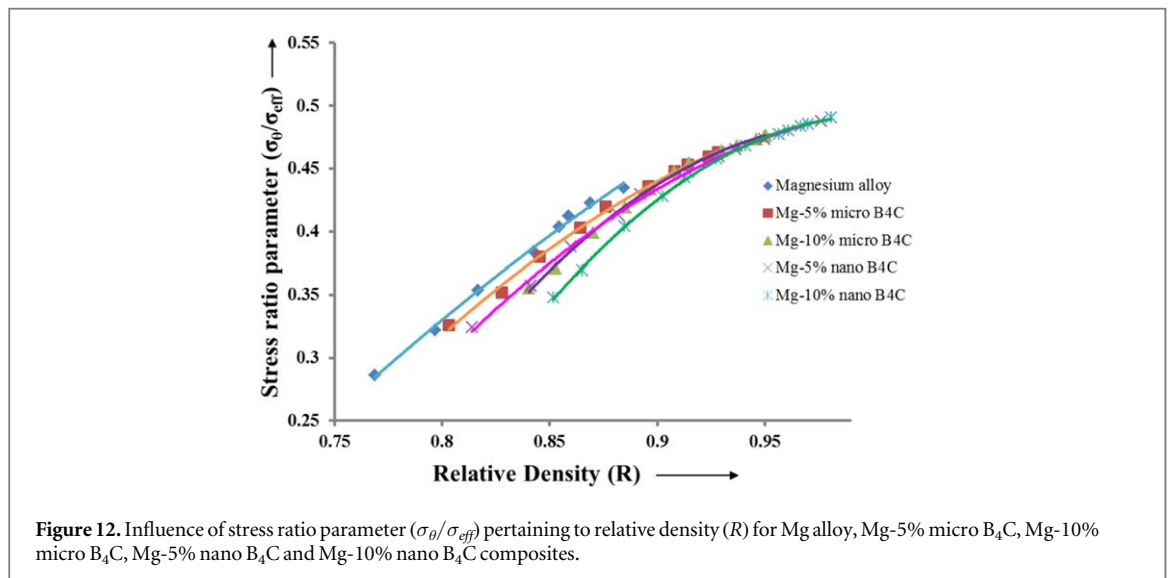


Figure 12. Influence of stress ratio parameter ($\sigma_{\theta}/\sigma_{eff}$) pertaining to relative density (R) for Mg alloy, Mg-5% micro B_4C , Mg-10% micro B_4C , Mg-5% nano B_4C and Mg-10% nano B_4C composites.

4.1.6. Influence of stress ratio parameters pertaining to relative density (R)

The stress ratio parameters ($\sigma_{\theta}/\sigma_{eff}$, σ_m/σ_{eff} & σ_z/σ_m) has been drawn against the relative density (R) for magnesium alloy and its composites containing 5% and 10% B_4C particles of micro and nano sizes by using parabolic curve fitting technique of second order polynomial equation as shown in the figures 12–14. The result shows that the mean stress (σ_m) and hoop stress (σ_{θ}) rises through the increase in relative density (R) as compared to effective stress (σ_{eff}). With gradual increase in the load during cold upsetting, the resistance against deformation increases due to the volume required to close the pores gets reduced. Therefore bulging takes place with increase in σ_{θ} & σ_m and hence the stress ratio parameters ($\sigma_{\theta}/\sigma_{eff}$ & σ_m/σ_{eff}) increase with increase in relative density (R). Since the relative density (R) is incremental, the stress ratio parameters ($\sigma_{\theta}/\sigma_{eff}$ & σ_m/σ_{eff}) increases compared with previous level which leads to formation of initial crack by damaging the pores on the composites. Composites with larger value of relative density yield the highest stress ratio parameters ($\sigma_{\theta}/\sigma_{eff}$ & σ_m/σ_{eff}). The relative density (R) of Mg-10% nano B_4C composite is higher than all other composites for the particular stress ratio parameters.

On the other hand, when the stress ratio parameter of (σ_z/σ_m) is drawn pertaining to relative density (R), the behaviour has been reversed. This is due to the compressive nature of the true axial stress (σ_z). The maximum and minimum values of stress ratio parameters ($\sigma_{\theta}/\sigma_{eff}$ & σ_m/σ_{eff}) are given in the table 7.

4.1.7. Influence of instantaneous strain hardening index (n_i) pertaining to relative density (R)

Graph shown in figure 15 has been drawn for the instantaneous strain hardening index (n_i) pertaining to relative density (R) for magnesium alloy and its composites containing 5% and 10% B_4C particles of micro and nano sizes as It has been observed that the instantaneous strain hardening index (n_i) drops rapidly with increase in

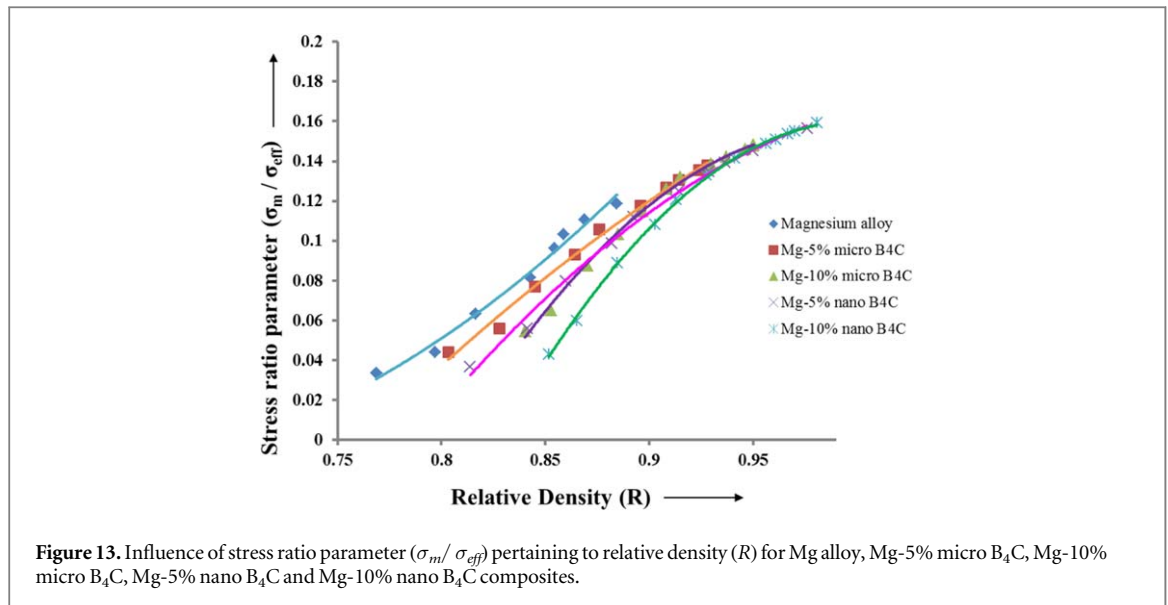


Figure 13. Influence of stress ratio parameter (σ_m / σ_{eff}) pertaining to relative density (R) for Mg alloy, Mg-5% micro B_4C , Mg-10% micro B_4C , Mg-5% nano B_4C and Mg-10% nano B_4C composites.

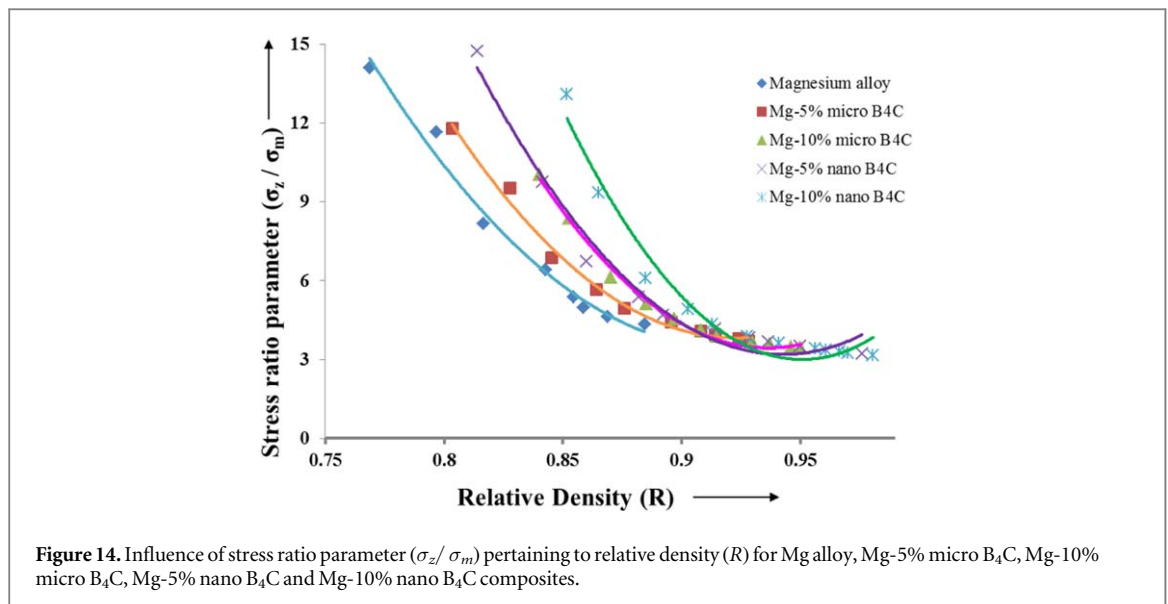
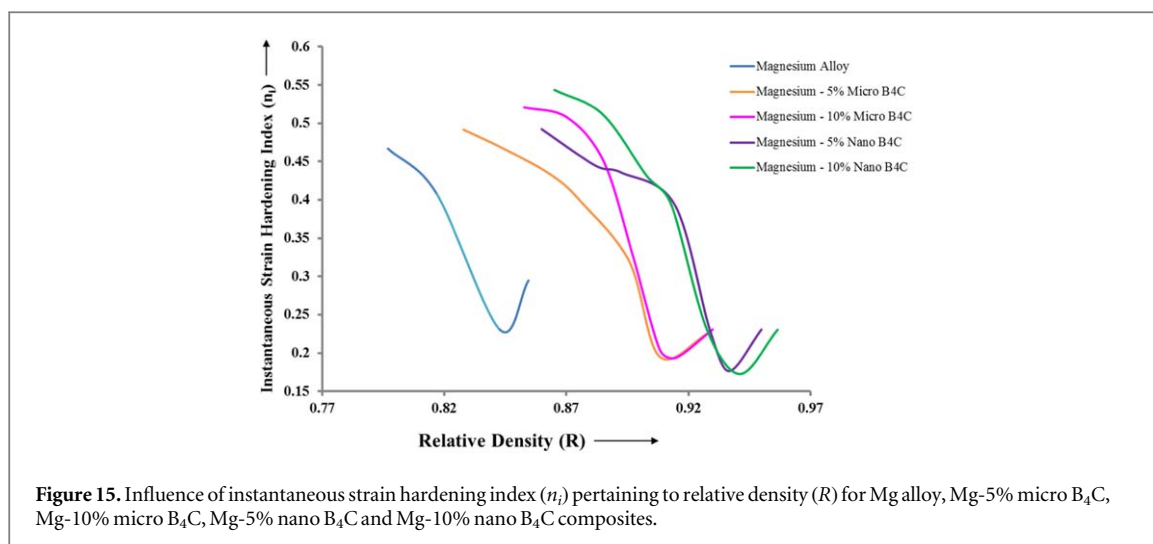


Figure 14. Influence of stress ratio parameter (σ_z / σ_m) pertaining to relative density (R) for Mg alloy, Mg-5% micro B_4C , Mg-10% micro B_4C , Mg-5% nano B_4C and Mg-10% nano B_4C composites.

Table 7. The maximum values Stress ratio parameters ($\sigma_\theta / \sigma_{eff}$ & σ_m / σ_{eff}) and minimum value of stress ratio parameters (σ_z / σ_m) for Mg alloy, Mg-5% micro B_4C , Mg-10% micro B_4C , Mg-5% nano B_4C and Mg-10% nano B_4C composites.

S. no.	Composites	Stress ratio parameters		
		$\sigma_\theta / \sigma_{eff}$ (Max. Value)	σ_m / σ_{eff} (Max. Value)	σ_z / σ_m (Min. Value)
1.	Mg alloy	0.4349	0.1186	4.3329
2.	Mg-5% micro B_4C	0.4629	0.1379	3.7125
3.	Mg-10% micro B_4C	0.4763	0.1482	3.4283
4.	Mg-5% nano B_4C	0.4876	0.1565	3.2325
5.	Mg-10% nano B_4C	0.4900	0.1593	3.1637

relative density from 0.79 to 0.84 in case of Mg alloy. For Mg-5% micro B_4C the drop takes place from the relative density 0.82 to 0.90 and for Mg-5% nano B_4C , it takes place from the relative density 0.86 to 0.93. Similarly for Mg-10% micro B_4C the drop takes place from the relative density 0.85 to 0.91 and for Mg-10% nano B_4C it takes place from the relative density 0.87 to 0.94. This is due to the phenomenon of pore closure during the load application. Hence the curve continues to decrease because of strain softening upto that relative density. Beyond that, with further increase in deformation the matrix work hardening increases and hence instantaneous strain hardening index (n_i) begins to increase slightly. It continues to rise up until the flow softening occurs towards the



end of deformation because of the influence of both geometrical as well matrix work hardening. As compared to Mg alloy, instantaneous strain hardening index (n_i) increases with the inclusion of B_4C particles and further increases with the reduction of its particle size.

5. Conclusion

The experimental investigation of formability and strain hardening index of the Mg alloy, Mg-5% micro B_4C , Mg-10% micro B_4C , Mg-5% nano B_4C and Mg-10% nano B_4C composites has been studied using cold deformation test and the following conclusions were made:

- The powder characterization of the composites through SEM confirms the presence of B_4C and its bonding with Mg alloy and the XRD and EDS results further confirms the existence of both Mg and B_4C in the composites with different peaks.
- It is evident that increasing the weight % of B_4C reinforcement reduces the porosity of composites. Further reducing the B_4C reinforcement particle size increases the densification of the composites because of the better load distribution. This leads to the higher formability index value (β_σ).
- The results of the cold upsetting reveals that increasing the B_4C particles increases the relative density (R) due to the low porosity. Among all the composites, Mg-10% nano B_4C composite has high strength and formability (β_σ) behaviour than other composites.
- Stress ratio parameters ($\sigma_\theta / \sigma_{eff}$ & σ_m / σ_{eff}) for Mg-10% nano B_4C composite is higher than the other composites due to the better densification and low porosity and the stress ratio parameter (σ_z / σ_m) decreases for the composites compared to Mg alloy because of the higher mean stress (σ_m) combined with low porosity.
- As compared to Mg alloy, the inclusion of the B_4C particles increases the instantaneous strain hardening index (n_i). This parameter further increases with reduced particle size of B_4C reinforcement due to the better load distribution and high densification.

ORCID iDs

C Kailasanathan  <https://orcid.org/0000-0002-4744-9548>

References

- [1] Sazonov MA, Chernyshova TA and Rokhlin LL 2013 Microstructure and mechanical properties of disperse reinforced composite material with AZ91 matrix alloy *Inorg. Mater. Appl. Res.* **4** 287–94
- [2] Kannan C and Ramanujam R 2017 Comparative study on the mechanical and microstructural characterization of AA 7075 nano and hybrid nanocomposites produced by stir and squeeze casting *J. Adv. Res.* **8** 309–19
- [3] Hu H, Yu A, Li N and Allison JE 2003 Potential magnesium alloys for high temperature die cast automotive applications: a review *Mater. Manuf. Process.* **18** 687–717

- [4] Friedrich H E and Mordike B L 2006 *Magnesium Technology: Metallurgy, Design Data, Applications* (Germany: Springer) Magnesium Technology: Metallurgy, Design Data, Applications Magnesium Technology: Metallurgy, Design Data, Applications Magnesium Technology: Metallurgy, Design Data, Applications (<https://doi.org/10.1007/3-540-30812-1>)
- [5] Jin Q, Tian G, Li J, Zhao Y and Yan H 2019 The study on corrosion resistance of superhydrophobic magnesium hydroxide coating on AZ31B magnesium alloy *Colloids and Surfaces A: Physicochemical and Engineering Aspects* **577** 8–16
- [6] Esen Z 2011 TiNiReinforced magnesium composites by powder metallurgy *Magnesium Technology* (Pittsburgh, PA: The Minerals, Metals & Materials Society.) **457–62** Magnesium Technology Magnesium Technology
- [7] Falcon-Franco L, Rosales I, García-Villarreal S, Curiel F F and Arizmendi-Orquecho A 2016 Synthesis of magnesium metallic matrix composites and the evaluation of aluminium nitride addition effect *J. Alloys Compd.* **663** 407–12
- [8] Dey A and Pandey K M 2015 Magnesium metal matrix composites—a review *Rev. Adv. Mater. Sci.* **42** 58–67 http://www.ipme.ru/e-journals/RAMS/no_14215/07_14215_dey.pdf
- [9] Suresh S, ShenbagaVinayagaMoorthi N, Vettivel S C and Selvakumar N 2014 Mechanical behavior and wear prediction of stir cast Al-TiB₂ composites using response surface methodology *Mater. Des.* **59** 383–96
- [10] Prasad K N P and Ramachandra M 2018 Determination of abrasive wear behaviour of al-fly ash metal matrix composites produced by squeeze casting *Materials Today: Proceedings* **5** 2844–53
- [11] Ghasali E, Alizadeh M, Niazmand M and Ebadzadeh T 2017 Fabrication of Magnesium-Boron carbide metal matrix composite by powder metallurgy route: comparison between microwave and spark plasma sintering *J. Alloys Compd.* **697** 200–7
- [12] Yao Y T, Jiang L, Fu G F and Chen L Q 2015 Wear behavior and mechanism of B₄C reinforced Mg-matrix composites fabricated by metal-assisted pressureless infiltration technique *Trans. Nonferrous Met. Soc. China (English Ed.)* **25** 2543–8
- [13] Domnich V, Reynaud S, Haber R A and Chhowalla M 2011 Boron carbide: structure, properties, and stability under stress *J. Am. Ceram. Soc.* **94** 3605–28
- [14] Lu R, Chandrasekaran S, Du Frane W L, Landingham R L, Worsley M A and Kuntz J D 2018 Complex shaped boron carbides from negative additive manufacturing *Mater. Des.* **148** 8–16
- [15] Rao S R and Padmanabhan G 2012 Fabrication and mechanical properties of aluminium-boron carbide composites, *Int J. Mater. Biomater. Appl.* **2** 15–8 <https://pdfs.semanticscholar.org/b356/7da1f9e348a63439b2bc529ef2de06217ace.pdf>
- [16] Chen L and Yao Y 2014 Processing, microstructures, and mechanical properties of magnesium matrix composites: a review *Acta Metall. Sin. (Engl. Lett.)* **27** 762–74
- [17] Rana H G, Badheka V J and Kumar A 2016 Fabrication of Al7075/B₄C surface composite by novel Friction Stir Processing (FSP) and investigation on wear *Procedia Technol.* **23** 519–28
- [18] Vettivel S C, Selvakumar N and Leema N 2013 Experimental and prediction of sintered Cu-W composite by using artificial neural networks *Mater. Des.* **45** 323–35
- [19] Varma Vijay K, Kumar S V, Mahajan Y R and Kutumbara V V 1998 Cyclic stress response of Al–Cu–Mg alloy matrix composites with SiCp of varying sizes *Scripta Mater* **38** 1571–5
- [20] Sridhar I and Fleck N A 2000 Yield behavior of cold compacted composite powders *Acta Mater.* **48** 3341–52
- [21] Szczepanik S and Lohnert W 1996 The formability of the Al–5% SiC composite obtained using P/M method *J. Mater. Process. Technol.* **60** 703–9
- [22] Selvakumar N, Mohan Raj A P and Narayanasamy R 2012 Experimental investigation on workability and strain hardening behaviour of Fe–C–0.5 Mn sintered composites *Mater. Des.* **41** 349–57
- [23] Narayan S and Rajeshkannan A 2014 ‘Workability behaviour of powder metallurgy aluminium composites *Journal of Powder Technology* **368721**
- [24] Narayanasamy R, Ramesh T and Pandey K S 2005 An investigation on instantaneous strain hardening behavior in three dimensions of aluminum–iron composites during cold upsetting *J Mater SciEng A* **394** 149–60
- [25] Narayanasamy R, Ramesh T and Pandey K S 2007 An experimental investigation on strain hardening behaviour of aluminium–3.5% alumina powder metallurgy composite preform under various stress states during cold upset forming *Mater. Des.* **28** 1211–23
- [26] Narayanasamy R, Ananthkrishnan V and Pandey K S 2008 Comparison of workability strain, stress parameters of powder metallurgy steels AISI 9840, and AISI 9845 during cold upsetting *Mater. Des.* **29** 1919–25
- [27] Narayanasamy R, Selvakumar N and Pandey K S 2007 Phenomenon of instantaneous strain hardening behavior of sintered Al–Fe composite preforms during cold axial forming *Mater. Des.* **28** 1358–63
- [28] Narayanasamy R, Ramesh T and Pandey K S 2006 Some aspects on strain hardening behavior in three dimensions of aluminum–iron powder metallurgy composite during cold upsetting *Mater. Des.* **27** 640–50
- [29] Jabbari-Taleghani M A and Torralba J M 2014 Hot workability of nanocrystalline AZ91 magnesium alloy *J. Alloys Compd.* **595** 1–7
- [30] Zhou S S, Deng K K, Li J C, Nie K B, Xu F J, Zhou H F and Fan J F 2014 Hot deformation behavior and workability characteristics of bimodal size SiCp/AZ91 magnesium matrix composite with processing map *Mater. Des.* **64** 177–84
- [31] Narayanasamy R, Senthilkumar V and Pandey K S 2006 Some aspects of workability studies on hot forging of sintered high strength 4% titanium carbide composite steel preforms *Mater. Sci. Eng. A* **425** 121–30
- [32] Narayanasamy R, Anandkrishnan V and Pandey K S 2008 Effect of geometric work-hardening and matrix work-hardening on workability and densification of aluminium-3.5% alumina composite during cold upsetting *Mater. Des.* **29** 1582–99
- [33] Mohan Raj A P and Selvakumar N 2011 Deformation Behavior of Sintered Fe-C-Mn Composite During Cold Upset Forming *Mater. Manuf. Process.* **26** 1388–92
- [34] Kannan A R, Pandey K S and Shanmugam S 2008 Some investigation on the cold deformation behaviour of sintered iron-0.8% carbon alloy powder preforms *J. Mater. Process. Technol.* **203** 542–7
- [35] Mohan Raj A P, Kailasanathan C and Seenikannan P 2014 Influence of carbon content on Workability and Density ratio of Sintered Iron Based Composites *International Journal of Chem. Tech, Research* **6** 4777–81 <https://pdfs.semanticscholar.org/b5f2/b7621f32313eaf79367a8155cb929dd6f440.pdf>
- [36] Narayanasamy R, Ramesh T and Prabhakar M 2009 Effect of particle size of SiC in aluminium matrix on workability and strain hardening behaviour of P/M composite *Mater. Sci. Eng. A* **504** 13–23
- [37] Seetharam R, Kanmani Subbu S and Davidson M J 2017 Hot workability and densification behavior of sintered powder metallurgy Al-B₄C preforms during upsetting *J. Manuf. Processes* **28** 309–18
- [38] Li H Z, Wei X Y, Ouyang J, Jiang J and Li Y 2013 Hot deformation behavior of extruded AZ80C magnesium alloy *Trans. Nonferrous Met. Soc. China (English Ed.)* **23** 3180–5
- [39] Narayanasamy P and Selvakumar N 2017 Tensile, compressive and wear behaviour of self-lubricating sintered magnesium based composites *Trans. Nonferrous Met. Soc. China (English Ed.)* **27** 312–23

- [40] Kannan R, Narayanan A, Ahmed Z, Prasad A and Narayan S 2019 Strain hardening analysis and modelling of its parameters for sintered Al and Al-1% C preforms during cold upsetting *Journal of Materials Research and Technology* **8** 1789–97
- [41] Ponraj N V, Azhagurajan A and Vettivel S C 2016 Microstructure, consolidation and mechanical behaviour of Mg/n-TiC composite *Alex. Engg. J.* **55** 2077–86
- [42] Vettivel S C, Selvakumar N, Leema N and Lenin A H 2014 Electrical resistivity, wear map and modeling of extruded tungsten reinforced copper composite *Mater. Des.* **56** 791–806
- [43] Mohan Raj A P, Selvakumar N, Narayanasamy R and Kailasanathan C 2013 Experimental investigation on workability and strain hardening behaviour of Fe–C–Mn sintered composites with different percentage of carbon and manganese content *Mater. Des.* **49** 791–801
- [44] Sumathi M, Selvakumar N and Narayanasamy R 2012 Workability studies on sintered Cu-10SiC preforms during cold axial upsetting *Mater. Des.* **39** 1–8
- [45] Narayanasamy R, Ramesh T and Pandey K S 2005 Some aspects on workability of aluminium–iron powder metallurgy composite during cold upsetting *Mater. Sci. Eng. A* **391** 418–26
- [46] Vujovic V and Shabaik A H 1986 A new workability criterion for ductile metals *J. Eng. Mater. Technol.* **108** 245–9